

¹ An optimal divergence constraint ratio with
² implementation using mixed FEM-Meshfree formulation

³ Wu Junchao^{a,*}, Chu Yingjie¹, Xu Yangtao^a, Wang Dongdong¹

^a Key Laboratory for Intelligent Infrastructure and Monitoring of Fujian Province, College
of Civil Engineering, Huaqiao University , Xiamen, Fujian, 361021, China

⁴ **Abstract**

This is the abstract.

⁵ *Keywords:* keyword1, keyword2, keyword3, keyword4, keyword5

*Corresponding author
Email address: jcwu@hqu.edu.cn (Wu Junchao)

6 **1. Introduction**

7 The divergence constraint is a condition imposed to better capture specific
8 properties, such as the volumetric constraint in incompressible elasticity or the
9 divergence constraint of heat flux in heat diffusion. Proper imposition of this
10 constraint is crucial for obtaining better numerical solutions; insufficient or ex-
11 cessive constraints can reduce the accuracy and stability of the solution.

12 The divergence constraint ratio, denoted as r , is often used to measure the
13 level of constraint. For incompressible elasticity problems, the constraint ratio
14 is defined as the total degrees of freedom (DOFs) of displacement divided by
15 the total DOFs of pressure. Ideally, the optimal constraint ratio should be
16 consistent with its governing partial differential equations. For example, in
17 the two-dimensional (2D) case, the optimal constraint ratio is 2, since there
18 are two governing equations for displacement and one for pressure. When the
19 constraint ratio is less than 2, the formulation suffers from volumetric locking,
20 while a constraint ratio greater than 2 can cause a coarse solution for pressure.
21 These observations have been summarized by pioneering work [1] as follows:

$$r = \frac{2n_u}{n_p}, \quad \begin{cases} r > 2 & \text{too few constraints} \\ r = 2 & \text{optimal} \\ r < 2 & \text{too many constraints} \\ r \leq 1 & \text{severe locking} \end{cases} \quad (1)$$

22 where n_u and n_p are the number of control nodes for displacement and pressure,
23 respectively. Classifying the locked status via the constraint ratio is straight-
24 forward but imprecise. For instance, the divergence constraint ratio can remain
25 2 while the pressure is discretized using continuous shape functions identical to
26 the displacement's approximation. However, volumetric locking still exists in
27 this formulation.

28 The inf-sup condition, also known as the Ladyzhenskay-Babuška-Brezzi (LBB)
29 condition [2, 3], is a more precise requirement for a locking-free formulation.
30 This condition is based on the mixed-formulation framework, and when the
31 inf-sup condition is satisfied, both the accuracy and stability of the mixed-
32 formulation can be ensured. However, verifying the inf-sup condition is non-
33 trivial. An eigenvalue problem can be established to check this condition nu-
34 merically [4, 5, 6, 7]. Analytically, Brezzi and Fortin proposed a two-level pro-
35 jection framework that always satisfies the inf-sup condition, allowing it to be
36 checked by identifying whether the formulation is included in this framework.
37 Both analytical and numerical methods to check the inf-sup condition are com-
38 plex, and the relationship between the constraint ratio and the inf-sup condition
39 remains unclear.

40 To address divergence constraint issues, adjusting the constraint ratio to an
41 appropriate level is commonly used and easily implemented. In traditional finite
42 element methods (FEM), this adjustment is carried out based on elements since
43 the DOFs are embedded in each element. Conventional FEM often exhibits
44 an over-constrained status. Reducing the approximation order of pressure in

45 mixed-formulation can alleviate the constraint burden, such as with the well-
46 known Q4P1 (4-node quadrilateral displacement element with 1-node piecewise
47 constant pressure element) and Q8P3. Globally, using continuous shape functions
48 to link the local pressure DOFs in each element can also reduce the total
49 number of pressure DOFs and increase the constraint ratio, such as with T6P3
50 (6-node triangular displacement element with 3-node continuous linear pressure
51 element) and Q9P4 (Taylor-Hood element) [8]. These schemes belong to the
52 mixed-formulation framework and can also be implemented through a projection
53 approach, where the pressure approximant is projected into a lower-dimensional
54 space. Examples include selective integration methods [9, 10], B-bar or F-bar
55 methods [11, 12, 13, 14, 15], pressure projection methods [16, 17], and the en-
56 hanced strain method [18]. Meanwhile, conventional 3-node triangular elements
57 arranged in a regular cross pattern can also reduce the dimension of the pressure
58 space [19]. It should be noted that not all of these methods can meet the inf-sup
59 condition despite alleviating volumetric locking and producing a good displace-
60 ment solution. Some methods, like Q4P1, show significant oscillation for the
61 pressure solution, known as spurious pressure mode or checkerboard mode [19].
62 In such cases, additional stabilization approaches, such as multi-scale stabiliza-
63 tion (VMS) [20, 21, 22, 23] or Galerkin/least-squares (GLS) [24], are required
64 to eliminate the oscillations in pressure.

65 Another class of FEM methods adjusts the constraint ratio by increasing the
66 displacement DOFs. For instance, based on 3-node triangular elements, Arnold
67 et al. used a cubic bubble function in each element to increase the displacement
68 DOFs, known as the MINI element [25, 26]. It has been shown that this method
69 belongs to the VMS framework [27], and its fulfillment of the inf-sup condition
70 can be analytically evidenced using the two-level projection framework [6]. The
71 Crouzeix-Raviart element [28] transfers the DOFs from the triangular vertices to
72 edges, increasing the constraint ratio since, for triangular topology, the number
73 of edges is greater than that of vertices. More details about FEM technology
74 for divergence constraint issues can be found in Refs. [1, 3, 29].

75 In the past two decades, various novel approximations equipped with global
76 smoothed shape functions, such as moving least-squares approximation [30], re-
77 producing kernel approximation [31], radial basis functions [32, 33], maximum-
78 entropy approximation [34], and NURBS approximation [35, 36], have been pro-
79 posed. In these approaches, the approximant pressure evaluated by the deriva-
80 tives of global continuous shape functions also maintains a constraint ratio of
81 2 in 2D incompressible elasticity problems. However, the corresponding results
82 still show lower accuracy caused by locking [37, 38]. Widely-used locking-free
83 technologies for FEM are introduced in these approaches to enhance their per-
84 formance. For example, Moutsanidis et al. employed selective integration and
85 B-bar, F-bar methods for reproducing kernel particle methods [39, 40]. Wang
86 et al. applied selective integration schemes with bubble-stabilized functions to
87 node-based smoothed particle FEM [41]. Elguedj et al. proposed the B-bar and
88 F-bar NURBS formulations for linear and nonlinear incompressible elasticity.
89 Chen et al. adopted the pressure projection approach for reproducing kernel
90 formulations for nearly-incompressible problems [42], which was later extended

91 to Stokes flow formulations by Goh et al. [43]. Bombarde et al. developed
92 a block-wise NURBS formulation for shell structures, eliminating locking via
93 pressure projection [44]. Most of these approximations offer better flexibility for
94 arranging DOFs since their shape function constructions are no longer element-
95 dependent. Huerta et al. proposed a reproducing kernel approximation with
96 divergence-free basis functions to avoid volumetric strain entirely [45], although
97 this approach is unsuitable for compressible cases. Wu et al. added extra dis-
98 placement DOFs in FEM elements to resolve the locking issue, constructing
99 local shape functions using generalized meshfree interpolation to maintain con-
100 sistency [46]. Vu-Huu et al. employed different-order polygonal finite element
101 shape functions to approximate displacement and pressure, embedding a bubble
102 function in each element for stabilization.

103 This work proposes a more precise optimal divergence constraint ratio and
104 implements a locking-free and stabilized mixed FEM-Meshfree formulation with
105 this optimal constraint ratio. Firstly, the inf-sup condition is derived in a new
106 form, showing that the inf-sup value equals the lowest non-zero eigenvalue of
107 dilatation stiffness. Subsequently, involving a complete polynomial space with
108 dimensions identical to DOFs, this inf-sup value can be bounded by a two-level
109 estimator. This estimator provides a strong link between the inf-sup value and
110 the pressure DOFs, making it possible to justify the locking status by counting
111 the pressure nodes. From this estimator, two key ratios, namely the locking
112 ratio and the stabilized ratio, are defined. If the constraint ratio exceeds the
113 locking ratio, the formulation will show severe locking. If the constraint ratio is
114 lower than the locking ratio but greater than the stabilized ratio, the displace-
115 ment solution is free from locking, but the pressure shows oscillation, known as
116 the spurious pressure mode, and the inf-sup condition is not satisfied. When
117 the constraint ratio is lower than the stabilized ratio, the formulation achieves
118 satisfactory results, and the inf-sup condition is fulfilled. The stabilized ratio is
119 preferable to the locking ratio, but determining the stabilized ratio is not trivial.
120 The locking ratio can be determined by the total DOFs of the entire system,
121 but the stabilized ratio relates to the topology of the pressure. Currently, the
122 stabilized ratio should be determined numerically. Consequently, these two con-
123 straint ratios are considered optimal, and you can choose the better one based
124 on your requirements. If you focus only on the displacement result, the locking
125 ratio is sufficient. If capturing the pressure behavior is the aim, the stabilized
126 ratio should be used. For checking a formulation's locking status, these two
127 optimal constraint ratios are more precise than rough constraint counting in a
128 continuous sense and easier than the inf-sup test.

129 Furthermore, a mixed FEM-Meshfree formulation is proposed to verify the
130 optimal constraint ratio. In this mixed formulation, the displacement is approx-
131 imated by traditional finite element methods, and the pressure is discretized by
132 reproducing kernel meshfree approximation. With the aid of global RK shape
133 functions, the pressure's DOFs can be adjusted arbitrarily without considering
134 approximation order and numerical integration issues. Accordingly, a bubble
135 meshing scheme is proposed to generate a specific number of pressure nodes,
136 maintaining the constraint ratio as optimal.

137 The remainder of this paper is organized as follows: Section 2 reviews the
138 mixed-formulation framework for incompressible elasticity and heat diffusion
139 problems. In Section 3, a novel estimator of the inf-sup value is developed, from
140 which the optimal divergence constraint ratio is obtained. Section 4 introduces
141 the mixed FEM-Meshfree formulation and its corresponding mesh generator.
142 Section 5 verifies the proposed optimal divergence constraint ratio using a set of
143 inf-sup tests and benchmark examples, studying error convergence and stability
144 properties for the mixed FEM-Meshfree approximation. Finally, the conclusions
145 are presented in Section 6.

146 **2. Mixed and penalty formulations for nearly-incompressible elastic-**
 147 **ity problems**

148 *2.1. Penalty formulation*

149 Consider a body $\Omega \in \mathbb{R}^{n_d}$ with boundary Γ in n_d -dimension, where the Γ_t
 150 and Γ_g denotes its natural boundary and essential boundary such that $\Gamma_t \cup \Gamma_g =$
 151 Γ , $\Gamma_t \cap \Gamma_g = \emptyset$. The corresponding governing equations are given by:

$$\begin{cases} \nabla \cdot \boldsymbol{\sigma} + \mathbf{b} = \mathbf{0} & \text{in } \Omega \\ \boldsymbol{\sigma} \cdot \mathbf{n} = \mathbf{t} & \text{on } \Gamma_t \\ \mathbf{u} = \mathbf{g} & \text{on } \Gamma_g \end{cases} \quad (2)$$

152 in which $\boldsymbol{\sigma}$ denotes to stress tensor and, for isotropic linear elastic material, can
 153 be expressed by:

$$\boldsymbol{\sigma}(\mathbf{u}) = 3\kappa\boldsymbol{\varepsilon}^v(\mathbf{u}) + 2\mu\boldsymbol{\varepsilon}^d(\mathbf{u}) \quad (3)$$

154 where $\boldsymbol{\varepsilon}^v$ and $\boldsymbol{\varepsilon}^d$ are the volumetric(dilatation) and deviatoric parts of strain
 155 tensor $\boldsymbol{\varepsilon}$, and these are evaluated by:

$$\boldsymbol{\varepsilon}^v(\mathbf{u}) = \frac{1}{3}\nabla \cdot \mathbf{u} \mathbf{1}, \quad \boldsymbol{\varepsilon}^d(\mathbf{u}) = \frac{1}{2}(\mathbf{u}\nabla + \nabla\mathbf{u}) - \boldsymbol{\varepsilon}^v, \quad \boldsymbol{\varepsilon}^v : \boldsymbol{\varepsilon}^d = 0 \quad (4)$$

156 where $\mathbf{1} = \delta_{ij}\mathbf{e}_i \otimes \mathbf{e}_j$ is second order identity tensor. κ, μ are the bulk modulus
 157 and shear modulus, and they can be represented by Young's modulus E and
 158 Poisson's ratio ν :

$$\kappa = \frac{E}{2(1-2\nu)}, \quad \mu = \frac{E}{2(1+\nu)} \quad (5)$$

159 And \mathbf{b} denotes to prescribed body force in Ω . \mathbf{t}, \mathbf{g} are prescribed traction and
 160 displacement on natural and essential boundaries respectively.

161 In accordance with Galerkin formulation, the displacement denoted by \mathbf{u}
 162 can be got by the following weak problem: Find $\mathbf{u} \in V$

$$\int_{\Omega} 2\mu\delta\boldsymbol{\varepsilon}^d : \boldsymbol{\varepsilon}^d d\Omega + \int_{\Omega} 3\kappa\delta\boldsymbol{\varepsilon}^v : \boldsymbol{\varepsilon}^v d\Omega = \int_{\Gamma_t} \delta\mathbf{u} \cdot \mathbf{t} d\Gamma + \int_{\Omega} \delta\mathbf{u} \cdot \mathbf{b} d\Omega, \quad \forall \delta\mathbf{u} \in V \quad (6)$$

163 where V is the spaces defined by $V = \{\mathbf{v} \in H^1(\Omega)^2 \mid \mathbf{v} = \mathbf{g}, \text{ on } \Gamma_g\}$. $\delta\mathbf{u}$ is the
 164 virtual counterpart of \mathbf{u} , and $\delta\boldsymbol{\varepsilon}^v$ and $\delta\boldsymbol{\varepsilon}^d$ are the corresponding volumetric and
 165 deviatoric strain evaluated by $\delta\mathbf{u}$.

166 In traditional finite element formulation, the entire domain Ω is discretized
 167 by a set of construct mesh with vertices $\{\mathbf{x}_I\}_{I=1}^{n_u}$ [1], where n_u is the total
 168 number of vertices. Then, the displacement and its virtual counterpart can
 169 be approximated by the nodal coefficient and shape functions at \mathbf{x}_I 's, the ap-
 170 proximated displacement and its virtual counterpart, namely $\mathbf{u}_h, \delta\mathbf{u}_h$ have the
 171 following form:

$$\mathbf{u}_h(\mathbf{x}) = \sum_{I=1}^{n_u} N_I(\mathbf{x})\mathbf{u}_I, \quad \delta\mathbf{u}_h(\mathbf{x}) = \sum_{I=1}^{n_u} N_I(\mathbf{x})\delta\mathbf{u}_I \quad (7)$$

¹⁷² where N_I and \mathbf{u}_I are the shape function and nodal coefficient tensor at node \mathbf{x}_I .
¹⁷³ Introducing Eq. (7) to weak form of Eq. (6) leads to the following Ritz-Galerkin
¹⁷⁴ problem: Find $\mathbf{u}_h \in V_h$,

$$\int_{\Omega} 2\mu\delta\boldsymbol{\varepsilon}_h^d : \boldsymbol{\varepsilon}_h^d d\Omega + \int_{\Omega} 3\kappa\delta\boldsymbol{\varepsilon}_h^v : \boldsymbol{\varepsilon}_h^v d\Omega = \int_{\Gamma_t} \delta\mathbf{u}_h \cdot \mathbf{t} d\Gamma + \int_{\Omega} \delta\mathbf{u}_h \cdot \mathbf{b} d\Omega, \quad \forall \delta\mathbf{u}_h \in V_h \quad (8)$$

¹⁷⁵ where the approximate spaces $V_h \subseteq V$,

$$V_h = \{\mathbf{v}_h \in (\text{span}\{N_I\}_{I=1}^{n_u})^2 | \mathbf{v}_h^h = \mathbf{g}, \text{ on } \Gamma_g\} \quad (9)$$

¹⁷⁶ For the arbitrariness of $\delta\mathbf{u}_h$, the above equation can be reduced by elimination
¹⁷⁷ of $\delta\mathbf{u}_I$'s as the following discrete equilibrium equation:

$$(2\mu\mathbf{K}^d + 3\kappa\mathbf{K}^v)\mathbf{d}^u = \mathbf{f} \quad (10)$$

¹⁷⁸ where \mathbf{K}^v and \mathbf{K}^d are the volumetric and deviatoric stiffness matrices, and
¹⁷⁹ their components has the following forms:

$$\mathbf{K}_{IJ}^v = \int_{\Omega} \mathbf{B}_I^{vT} \mathbf{B}_J^v d\Omega \quad (11)$$

$$\mathbf{K}_{IJ}^d = \int_{\Omega} \mathbf{B}_I^{dT} \mathbf{B}_J^d d\Omega \quad (12)$$

¹⁸⁰ with and \mathbf{f} is the force vector and its components can be expressed by:

$$\mathbf{f}_I = \int_{\Gamma_t} N_I \mathbf{t} d\Gamma + \int_{\Omega} N_I \mathbf{b} d\Omega \quad (13)$$

¹⁸¹ \mathbf{d}^u is the coefficient vector containing \mathbf{u}_I 's.

¹⁸² It can be observed from Eq. (34) that, for a nearly-incompressible material,
¹⁸³ i.e. $\nu \rightarrow 0.5$, $\kappa \rightarrow \infty$. As a result, the volumetric stiffness matrix \mathbf{K}^v of (11)
¹⁸⁴ services as an enforcement like penalty method to enforce the volumetric deformation
¹⁸⁵ to be zero, $\nabla \cdot \mathbf{u} = 0$, while the bulking modulus κ can be regarded as
¹⁸⁶ a penalty parameter. Traditional finite element formulations suffer severe volumetric
¹⁸⁷ locking due to this enforcement, and this is so-called volumetric locking.
¹⁸⁸ To reduce the burden of volumetric locking, the reduced the integration points
¹⁸⁹ in volumetric stiffness matrix. For clarity, substituting numerical integration to
¹⁹⁰ the volumetric part of weak form in Eq. (8) leads to:
¹⁹¹

$$\int_{\Omega} 3\kappa\delta\boldsymbol{\varepsilon}_h^v : \boldsymbol{\varepsilon}_h^v d\Omega \approx \sum_{C=1}^{n_e} \sum_{G=1}^{n_g} 3\kappa \nabla \cdot \delta\mathbf{u}_h(\mathbf{x}_G) \nabla \cdot \mathbf{u}_h(\mathbf{x}_G) w_G \quad (14)$$

¹⁹² The corresponding components of volumetric stiffness \mathbf{K}^v in Eq. (11) yields:

$$\mathbf{K}_{IJ}^v \approx \bar{\mathbf{K}}_{IJ}^v = \sum_{C=1}^{n_e} \sum_{G=1}^{n_g} \mathbf{B}_I^{vT}(\mathbf{x}_G) \mathbf{B}_J^v(\mathbf{x}_G) w_G \quad (15)$$

193 where \mathbf{x}_G 's and w_G 's are the positions and weights of integration points. n_g is
 194 the total number of integration points in each element, thus the total integration
 195 point is $n_c \times n_g$. The reduced integration formulations use less number of inte-
 196 gration points compared with traditional full integration scheme. For instance,
 197 the conventional quadrilateral element use 2×2 Gauss integration points as
 198 full integration, the full integration means that the stiffness matrix is exactly
 199 evaluated by this integration scheme. And for reduced integration formulation,
 200 the number of integration points is reduced from 4 to 1.

201 *2.2. Mixed formulation*

202 Another approach to alleviate the volumetric locking is using the mixed-
 203 formulation. In this approach, the pressure is approximated by another way as
 204 follows:

$$\boldsymbol{\sigma}(\mathbf{u}, p) = p\mathbf{1} + 2\mu\boldsymbol{\varepsilon}^d(\mathbf{u}) \quad (16)$$

205 The strong form for mixed-formulation can be rephrased as:

$$\begin{cases} \nabla \cdot \boldsymbol{\sigma} + \mathbf{b} = \mathbf{0} & \text{in } \Omega \\ \frac{p}{\kappa} + \nabla \cdot \mathbf{u} = 0 & \text{in } \Omega \\ \boldsymbol{\sigma} \cdot \mathbf{n} = \mathbf{t} & \text{on } \Gamma_t \\ \mathbf{u} = \mathbf{g} & \text{on } \Gamma_g \end{cases} \quad (17)$$

206 where $p \in Q$, $Q = \{q \in L^2(\Omega) | \int_{\Omega} q d\Omega = 0\}$.

207 In traditional mixed formulations, the pressure p are discretized by different
 208 sets of controlled nodes, namely displacement nodes $\{\mathbf{x}_I\}_{I=1}^{n_d}$ and pressure nodes
 209 $\{\mathbf{x}_K\}_{K=1}^{n_p}$, where n_d and n_p are the total number of displacement nodes and
 210 pressure nodes. And then the approximate displacement denoted by \mathbf{u}_h and
 211 approximate pressure denoted by p_h can be expressed by

$$p_h(\mathbf{x}) = \sum_{K=1}^{n_p} \Psi_K(\mathbf{x}) p_K, \quad \delta p_h(\mathbf{x}) = \sum_{K=1}^{n_p} \Psi_K(\mathbf{x}) \delta p_K \quad (18)$$

212 where p_K 's are the coefficients. and N_I^d , N_K^p are the corresponding shape func-
 213 tions. the corresponding Ritz-Galerkin problem is that: Find $\mathbf{u}_h \in V_h$, $p_h \in Q_h$

214

$$\int_{\Omega} 2\mu\delta\boldsymbol{\varepsilon}_h^d : \boldsymbol{\varepsilon}_h^d d\Omega + \int_{\Omega} \nabla \cdot \delta\mathbf{u}_h p_h d\Omega = \int_{\Gamma_t} \delta\mathbf{u}_h \cdot \mathbf{t} d\Gamma + \int_{\Omega} \delta\mathbf{u}_h \cdot \mathbf{b} d\Omega, \quad \forall \delta\mathbf{u}_h \in V_h \quad (19a)$$

$$\int_{\Omega} \delta p_h \nabla \cdot \mathbf{u}_h d\Omega - \int_{\Omega} \frac{1}{3\kappa} \delta p_h p_h d\Omega = 0, \quad \forall \delta p_h \in Q_h \quad (19b)$$

215 where $Q_h \subseteq Q$ are defined by:

$$Q_h = \{q_h \in \text{span}\{\Psi_K\}_{K=1}^{n_p} | \int_{\Omega} q_h d\Omega = 0\} \quad (20)$$

²¹⁶ With the arbitrariness of \mathbf{v}_h and q_h , the Eq.(??) leads to the following dis-
²¹⁷ crete governing equations:

$$\begin{bmatrix} 2\mu \mathbf{K}^{uu} & \mathbf{K}^{up} \\ (\mathbf{K}^{up})^T & -\frac{1}{3\kappa} \mathbf{K}^{pp} \end{bmatrix} \begin{Bmatrix} \mathbf{d}^u \\ \mathbf{d}^p \end{Bmatrix} = \begin{Bmatrix} \mathbf{f} \\ \mathbf{0} \end{Bmatrix} \quad (21)$$

²¹⁸ where $\mathbf{K}^{uu} = \mathbf{K}^d$.

²¹⁹ From the second equation of governing equilibrium equations in Eq. (21),
²²⁰ the coefficient vector \mathbf{d}^p can be expressed by \mathbf{d}^u as follows:

$$\mathbf{d}^p = 3\kappa(\mathbf{K}^{pp})^{-1}(\mathbf{K}^{up})^T \mathbf{d}^u \quad (22)$$

²²¹ Further substituting the above equation into first equation of Eq. (21) leads to:

$$\begin{aligned} (2\mu \underbrace{\mathbf{K}^{uu}}_{\mathbf{K}^d} + 3\kappa \underbrace{\mathbf{K}^{up}(\mathbf{K}^{pp})^{-1}(\mathbf{K}^{up})^T}_{\tilde{\mathbf{K}}^v}) \mathbf{d}^u &= \mathbf{f} \\ \Rightarrow (2\mu \mathbf{K}^d + 3\kappa \tilde{\mathbf{K}}^v) &= \mathbf{f} \end{aligned} \quad (23)$$

²²² 2.3. Equivalence between penalty- and mixed-formulation

²²³ It can be observed from the weak form for mixed-formulation in Eq. (19b)
²²⁴ or the discrete equation shown in Eq. (23) that, the solution of pressure p_h
²²⁵ is an orthogonal projection of $3\kappa \nabla \cdot \mathbf{u}_h$. Let $P_h : V_h \rightarrow P_h(V_h)$ such that
²²⁶ $P_h(V_h) \subseteq Q_h$, where $P_h(V_h) = \text{Im } P_h$ is the image of linear operator P_h [47].
²²⁷ Under this circumstance, $p_h = P_h(3\kappa \nabla \cdot \mathbf{u}_h) = 3\kappa \tilde{\nabla} \cdot \mathbf{u}_h$, and the Eq. (19b) can
²²⁸ be rephrased as:

$$\int_{\Omega} q_h (\nabla \cdot \mathbf{u}_h - \tilde{\nabla} \cdot \mathbf{u}_h) d\Omega = 0, \quad \forall q_h \in Q_h \quad (24)$$

²²⁹ Accordingly, the corresponding volumetric part of weak form turns to:

$$\begin{aligned} \int_{\Omega} \nabla \cdot \delta \mathbf{u}_h p_h d\Omega &= \underbrace{\int_{\Omega} (\nabla \cdot \mathbf{u}_h - \tilde{\nabla} \cdot \delta \mathbf{u}_h) p_h d\Omega}_0 + \int_{\Omega} \tilde{\nabla} \cdot \delta \mathbf{u}_h \underbrace{p_h}_{\tilde{\nabla} \cdot \mathbf{u}_h} d\Omega \\ &= \int_{\Omega} 3\kappa \tilde{\nabla} \cdot \delta \mathbf{u}_h \tilde{\nabla} \cdot \mathbf{u}_h d\Omega \end{aligned} \quad (25)$$

²³⁰ and the Ritz-Galerkin formulation becomes to: Find $\mathbf{u}_h \in V_h$

$$\int_{\Omega} 2\mu \delta \mathbf{e}_h^d : \mathbf{e}_h^d d\Omega + \int_{\Omega} 3\kappa \tilde{\nabla} \cdot \delta \mathbf{u}_h \tilde{\nabla} \cdot \mathbf{u}_h d\Omega = \int_{\Gamma_t} \delta \mathbf{u}_h \cdot \mathbf{t} d\Gamma + \int_{\Omega} \delta \mathbf{u}_h \cdot \mathbf{b} d\Omega, \quad \forall \mathbf{u}_h \in V_h \quad (26)$$

²³¹ In contrast, for penalty formulation, the reduced numerical integration also
²³² can be regarded as a projection. Let ϱ_i be the orthogonal polynomials,

$$\int_{\Omega_C} \varrho_i \varrho_j d\Omega = \begin{cases} J_C w_i & i = j \\ 0 & i \neq j \end{cases} \quad (27)$$

²³³ The orthogonal interpolation $T^k : V \rightarrow W^k$, where W^k is the interpolation
²³⁴ space spanned by k orthogonal polynomials:

$$W^k := \text{span}\{\varrho_i\}_{i=1}^k \quad (28)$$

²³⁵ For traditional Gauss-type integration scheme, $\varrho_i(\mathbf{x}_j) = \delta_{ij}$, \mathbf{x}_j 's are the positions
²³⁶ of integration points. The volumetric strain can be depicted by orthogonal
²³⁷ interpolation as:

$$\nabla \cdot \mathbf{u}_h(\mathbf{x}) \approx \bar{\nabla} \cdot \mathbf{u}_h(\mathbf{x}) = \sum_{G=1}^{n_g} \varrho_G(\mathbf{x}) \nabla \cdot \mathbf{u}_h(\mathbf{x}_G), \quad \nabla \cdot \mathbf{u}_h(\mathbf{x}_G) = \bar{\nabla} \cdot \mathbf{u}_h(\mathbf{x}_G) \quad (29)$$

²³⁸ while the integration points are regarded as interpolation coefficients. While
²³⁹ the total number of integration points n_g is lower than full integration, these
²⁴⁰ means $\nabla \cdot \mathbf{u}_h$ projects to a subspace.

$$\begin{aligned} \int_{\Omega} 3\kappa \bar{\nabla} \cdot \delta \mathbf{u}_h \bar{\nabla} \cdot \mathbf{u}_h d\Omega &= \sum_{C=1}^{n_e} \sum_{G,L=1}^{n_g} 3\kappa \nabla \cdot \delta \mathbf{u}_h(\mathbf{x}_G) \nabla \cdot \mathbf{u}_h(\mathbf{x}_L) \int_{\Omega} \varrho_G \varrho_L d\Omega \\ &= \sum_{C=1}^{n_e} \sum_{G=1}^{n_g} 3\kappa \nabla \cdot \delta \mathbf{u}_h(\mathbf{x}_G) \nabla \cdot \mathbf{u}_h(\mathbf{x}_G) J_C w_G \end{aligned} \quad (30)$$

²⁴¹ With comparison of Eqs. (30) and (25), the penalty formulation is actually
²⁴² equivalence with mixed formulation that, all approaches can be described by
²⁴³ projection format.

²⁴⁴ **3. Mixed-formulation**

²⁴⁵ *3.1. Nearly-incompressible elasticity*

²⁴⁶ Consider a body $\Omega \in \mathbb{R}^{n_d}$ with boundary Γ in n_d -dimension, where the Γ_t
²⁴⁷ and Γ_g denotes its natural boundary and essential boundary such that $\Gamma_t \cup \Gamma_g =$
²⁴⁸ Γ , $\Gamma_t \cap \Gamma_g = \emptyset$. The corresponding governing equations for mixed-formulation
²⁴⁹ are given by:

$$\begin{cases} \nabla \cdot \boldsymbol{\sigma} + \mathbf{b} = \mathbf{0} & \text{in } \Omega \\ \frac{p}{\kappa} + \nabla \cdot \mathbf{u} = 0 & \text{in } \Omega \\ \boldsymbol{\sigma} \cdot \mathbf{n} = \mathbf{t} & \text{on } \Gamma_t \\ \mathbf{u} = \mathbf{g} & \text{on } \Gamma_g \end{cases} \quad (31)$$

²⁵⁰ where \mathbf{u} and p , stand for displacement and hydrostatic pressure respectively, are
²⁵¹ the variables of this problem. $\boldsymbol{\sigma}$ denotes to stress tensor and has the following
²⁵² form:

$$\boldsymbol{\sigma}(\mathbf{u}, p) = p\mathbf{1} + 2\mu\nabla^s \mathbf{u} \quad (32)$$

²⁵³ in which $\mathbf{1} = \delta_{ij}\mathbf{e}_i \otimes \mathbf{e}_j$ is second order identity tensor. $\boldsymbol{\varepsilon}$ and $\text{tr } \boldsymbol{\varepsilon}$ are strain
²⁵⁴ tensor and its trace counterpart evaluated by:

$$\nabla^s \mathbf{u} = \frac{1}{2}(\mathbf{u}\nabla + \nabla\mathbf{u}) - \frac{1}{3}\boldsymbol{\varepsilon} : \mathbf{1} \quad (33)$$

²⁵⁵ and κ, μ are the bulk modulus and shear modulus, and they can be represented
²⁵⁶ by Young's modulus E and Poisson's ratio ν :

$$\kappa = \frac{E}{2(1-2\nu)}, \quad \mu = \frac{E}{2(1+\nu)} \quad (34)$$

²⁵⁷ Moreover, \mathbf{b} denotes to prescribed body force in Ω . \mathbf{t}, \mathbf{g} are prescribed
²⁵⁸ traction and displacement on natural and essential boundaries respectively.

²⁵⁹ In accordance with Galerkin formulation, the weak form can be given by:
²⁶⁰ Find $\mathbf{u} \in V, p \in Q$,

$$\begin{aligned} a(\mathbf{v}, \mathbf{u}) + b(\mathbf{v}, p) &= f(\mathbf{v}) & \forall \mathbf{v} \in V \\ b(\mathbf{u}, q) &= \mathbf{0} & \forall q \in Q \end{aligned} \quad (35)$$

²⁶¹ with the spaces V, Q defined by:

$$V = \{\mathbf{v} \in H^1(\Omega)^2 \mid \mathbf{v} = \mathbf{g}, \text{ on } \Gamma_g\} \quad (36)$$

$$Q = \{q \in L^2(\Omega) \mid \int_{\Omega} q d\Omega = 0\} \quad (37)$$

²⁶³ where $a : V \times V \rightarrow \mathbb{R}$ and $b : V \times Q \rightarrow \mathbb{R}$ are bilinear form, and $f : V \rightarrow \mathbb{R}$ is
²⁶⁴ the linear form. In elasticity problem, they has the following forms:

$$a(\mathbf{v}, \mathbf{u}) = \int_{\Omega} \nabla^s \mathbf{v} : \nabla^s \mathbf{u} d\Omega \quad (38)$$

$$b(\mathbf{v}, q) = \int_{\Omega} \nabla \cdot \mathbf{v} q d\Omega \quad (39)$$

$$f(\mathbf{v}) = \int_{\Gamma_t} \mathbf{v} \cdot \mathbf{t} d\Gamma + \int_{\Omega} \mathbf{v} \cdot \mathbf{b} d\Omega \quad (40)$$

²⁶⁷ *3.2. Heat diffusion*

²⁶⁸ Another traditional mixed-formulation problem considered in this work is
²⁶⁹ heat diffusion problem, while the problem domain denotes to $\Omega \in \mathbb{R}^{n_d}$ with
²⁷⁰ boundary Γ . The strong form of this problem is given by:

$$\begin{cases} \nabla \cdot \mathbf{p} + b = 0 & \text{in } \Omega \\ \mathbf{p} + \nabla u = 0 & \text{in } \Omega \\ \mathbf{p} \cdot \mathbf{n} = t & \text{on } \Gamma_t \\ u = g & \text{on } \Gamma_g \end{cases} \quad (41)$$

²⁷¹ The corresponding weak formulation can be stated as:

$$\begin{aligned} a(\mathbf{q}, \mathbf{p}) + b(\mathbf{q}, u) &= \mathbf{0} & \forall \mathbf{q} \in Q \\ b(\mathbf{p}, v) &= g(v) & \forall v \in V \end{aligned} \quad (42)$$

²⁷² **4. Optimal polynomial-wise constraint ratio**

²⁷³ *4.1. Inf-sup value estimator*

²⁷⁴ Without loss generality, the incompressible elasticity problem is considered
²⁷⁵ herein to illustrate the proposed methodology. The approximations of Eq.(??)
²⁷⁶ should satisfy the inf-sup condition, or as known Ladyzhenskaya–Babuška–
²⁷⁷ Brezzi condition [3], to ensure the formulation's accuracy:

$$\inf_{q_h \in Q_h} \sup_{\mathbf{v}_h \in V_h} \frac{|b(q_h, \mathbf{v}_h)|}{\|q_h\|_Q \|\mathbf{v}_h\|_V} \geq \beta > 0 \quad (43)$$

²⁷⁸ in which β , namely inf-sup value, is a constant independent of characterized
²⁷⁹ element size h .

²⁸⁰ **Theorem 1.** Suppose $\mathcal{P}_h : V_h \rightarrow Q_h$ is the orthogonal projection operator of \mathcal{P}
²⁸¹ defined by:

$$b(q_h, \mathbf{v}_h) = (q_h, \mathcal{P}_h \mathbf{v}_h) = (q_h, \mathcal{P}_h \mathbf{v}_h), \quad \forall q_h \in Q_h \quad (44)$$

²⁸² where $\mathcal{P} : V \rightarrow Q$ is the divergence operator, $\mathcal{P} = \nabla \cdot$. And the inf-sup value can
²⁸³ be estimated by:

$$\beta \leq \inf_{V'_h \subset V_h \setminus \ker \mathcal{P}_h} \sup_{\mathbf{v}_h \in V'_h} \frac{\|\mathcal{P}_h \mathbf{v}_h\|_Q}{\|\mathbf{v}_h\|_V} \quad (45)$$

²⁸⁴ where $\ker \mathcal{P}_h \subset V$ is the kernel of \mathcal{P}_h defined by $\ker \mathcal{P}_h := \{\mathbf{v} \in V \mid \mathcal{P}_h \mathbf{v} = 0\}$.

²⁸⁵ PROOF. As the definition of \mathcal{P}_h , we have $\text{Im} \mathcal{P}_h \in Q_h$. And the Eq. (43) can be
²⁸⁶ rewritten as:

$$\beta \leq \inf_{q_h \in Q_h} \sup_{\mathbf{v}_h \in V_h} \frac{|b(q_h, \mathbf{v}_h)|}{\|q_h\|_Q \|\mathbf{v}_h\|_V} \leq \inf_{q_h \in \text{Im} \mathcal{P}_h} \sup_{\mathbf{v}_h \in V_h} \frac{|(q_h, \mathcal{P}_h \mathbf{v}_h)|}{\|q_h\|_Q \|\mathbf{v}_h\|_V} \quad (46)$$

²⁸⁷ For a given $q_h \in \text{Im} \mathcal{P}_h$, suppose a space $V'_h \subset V_h \setminus \ker \mathcal{P}_h$ defined by:

$$V'_h = \{\mathbf{v}_h \in V_h \mid \mathcal{P}_h \mathbf{v}_h = q_h\} \quad (47)$$

²⁸⁸ Since $\text{Im} \mathcal{P}_h \in Q_h$, in accordance with Cauchy-Schwarz inequality, we have:

$$|(q_h, \mathcal{P}_h \mathbf{v}_h)| \leq \|q_h\|_Q \|\mathcal{P}_h \mathbf{v}_h\|_Q \quad (48)$$

²⁸⁹ where this equality is holding if and only if $q_h = \mathcal{P}_h \mathbf{v}_h$, i.e.,

$$|(q_h, \mathcal{P}_h \mathbf{v}_h)| = \|q_h\|_Q \|\mathcal{P}_h \mathbf{v}_h\|_Q, \quad \forall \mathbf{v}_h \in V'_h \quad (49)$$

²⁹⁰ And the following relationship can be evidenced:

$$\sup_{\mathbf{v}_h \in V_h} \frac{|(q_h, \mathcal{P}_h \mathbf{v}_h)|}{\|q_h\|_Q \|\mathbf{v}_h\|_V} = \sup_{\mathbf{v}_h \in V'_h} \frac{\|\mathcal{P}_h \mathbf{v}_h\|_Q}{\|\mathbf{v}_h\|_V} \quad (50)$$

²⁹¹ Consequently, with a combination of Eqs. (46) and (50), Eq. (45) can be
²⁹² obtain.

293 **Remark 1.** *Theorem 1 is consistence with the traditional numerical inf-sup*
294 *test [4], while, according to minimum-maximum principle [48], the Eq. (45)*
295 *evaluates the general non-zero eigenvalue of metrics \mathbf{K}^v and \mathbf{K}^d .*

296 In order to further figure out the optimal constraint counting ,

297 **Theorem 2.** *Suppose that P_{n_u} is a polynomial space with n_u dimensions, and*
298 *V_{n_u} is the polynomial displacement space, $V_{n_u} = P_{n_u}^2$. The optimal dofs of*
299 *pressure n_p is equal to $n_c = \dim(V_{n_c} \setminus \ker \mathcal{P})$.*

300 PROOF. As the dimensions of V_h and V_{n_u} is identical, $\dim V_{n_u} = \dim V_h =$
301 $n_d \times n_u$. There exists a unique $\mathbf{v} \in V_{n_u}$ satisfying $\mathbf{v}_h = \mathcal{I}_h \mathbf{v}$. And the right side
302 of Eq. (45) becomes:

$$\inf_{V'_h \subset V_h \setminus \ker \mathcal{P}_h} \sup_{\mathbf{v}_h \in V'_h} \frac{\|\mathcal{P}_h \mathbf{v}_h\|_Q}{\|\mathbf{v}_h\|_V} = \inf_{V' \subset V_{n_u} \setminus \ker \mathcal{P}_h \mathcal{I}_h} \sup_{\mathbf{v} \in V'} \frac{\|\mathcal{P}_h \mathcal{I}_h \mathbf{v}\|_Q}{\|\mathcal{I}_h \mathbf{v}\|_V} \quad (51)$$

303 In accordance with triangular inequality, Cauchy-Schwarz inequality and the
304 relationship of Eqs. (44), we have:

$$\begin{aligned} \|\mathcal{P}_h \mathcal{I}_h \mathbf{v}\|_Q &= \sup_{q_h \in Q_h} \frac{|(q_h, \mathcal{P}_h \mathcal{I}_h \mathbf{v})|}{\|q_h\|_Q} = \sup_{q_h \in Q_h} \frac{|(q_h, \mathcal{P} \mathcal{I}_h \mathbf{v})|}{\|q_h\|_Q} \\ &\leq \sup_{q_h \in Q_h} \frac{|(q_h, \mathcal{P} \mathbf{v})| + |(q_h, \mathcal{P} \mathbf{v} - \mathcal{P} \mathcal{I}_h \mathbf{v})|}{\|q_h\|_Q} \\ &= \|\mathcal{P}_h \mathbf{v}\|_Q + \|\mathcal{P}(\mathcal{I} - \mathcal{I}_h)\mathbf{v}\|_Q \\ &\leq C \|\mathcal{P} \mathbf{v}\|_Q + \|\mathcal{P}(\mathcal{I} - \mathcal{I}_h)\mathbf{v}\|_Q \end{aligned} \quad (52)$$

305 Obviously, the second and third terms on the right side of Eq. (52) are the
306 interpolation error and the orthogonal projection error for approximations in
307 V_h , and can be evaluated by [49]:

$$\|\mathcal{P}(\mathcal{I} - \mathcal{I}_h)\mathbf{v}\|_Q \leq Ch^k |\mathbf{v}|_{H^k} \quad (53)$$

308 It can be obtained that $\|\mathcal{I}_h \mathbf{v}\|_V \geq C \|\mathbf{v}\|_V$ from close graph theorem [27]. And
309 considering it with Eqs. (52)-(53), the right side of Eq. (51) can be represented
310 as:

$$\begin{aligned} \inf_{V' \subset V_{n_u} \setminus \ker \mathcal{P}_h \mathcal{I}_h} \sup_{\mathbf{v} \in V'} \frac{\|\mathcal{P}_h \mathcal{I}_h \mathbf{v}\|_Q}{\|\mathcal{I}_h \mathbf{v}\|_V} &\leq \inf_{V' \subset V_{n_u} \setminus \ker \mathcal{P}_h \mathcal{I}_h} \sup_{\mathbf{v} \in V'} \frac{\|\mathcal{P}_h \mathbf{v}\|_Q}{\|\mathbf{v}\|_V} + Ch^k \\ &\leq C \inf_{V' \subset V_{n_u} \setminus \ker \mathcal{P}_h \mathcal{I}_h} \sup_{\mathbf{v} \in V'} \frac{\|\mathcal{P} \mathbf{v}\|_Q}{\|\mathbf{v}\|_V} + Ch^k \end{aligned} \quad (54)$$

311 Substituting Eqs. (51),(54) into (45) can get the following relationship:

$$\begin{aligned} \beta &\leq \beta_1 + Ch^k \\ &\leq C\beta_2 + Ch^k \end{aligned} \quad (55)$$

312 where

$$\beta_1 = \inf_{V' \subset V_{n_u} \setminus \ker \mathcal{P}_h \mathcal{I}_h} \sup_{\mathbf{v} \in V'} \frac{\|\mathcal{P}_h \mathbf{v}\|_Q}{\|\mathcal{I}_h \mathbf{v}\|_V} \quad (56)$$

$$\beta_2 = \inf_{V' \subset V_{n_u} \setminus \ker \mathcal{P}_h \mathcal{I}_h} \sup_{\mathbf{v} \in V'} \frac{\|\mathcal{P}\mathbf{v}\|_Q}{\|\mathbf{v}\|_V} \quad (57)$$

(58)

As illustrated in Figure ??, due to the approximations' partition of unity property, the sub-spaces $\ker \mathcal{P}$, $\ker \mathcal{P}_h$ and $\ker \mathcal{P}_h \mathcal{I}_h$ is arranged gathering at one side on V_{n_u} , where $n_p = \dim(V_{n_u} \setminus \ker \mathcal{P}_h \mathcal{I}_h) \leq n_d \times n_u$. Let $n_c = \dim(V_{n_u} \setminus \ker \mathcal{P})$, $n_h = \dim(V_{n_u} \setminus \ker \mathcal{P} \mathcal{I}_h)$, it is obvious that $\ker \mathcal{P} \subseteq \ker \mathcal{P} \mathcal{I}_h$, $n_h \leq n_c$. The different choices of n_p will appear the following three cases:

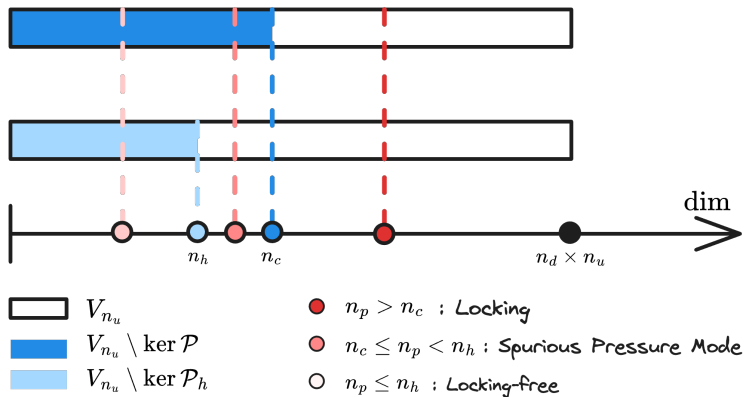


Figure 1: Illustration for optimal DOFs for pressure

- As $n_p > n_c$, there must exists a subspace in space $V_{n_u} \ker \mathcal{P}_h \mathcal{I}_h$ belong to $\ker \mathcal{P}$, resulting $\beta_2 = 0$. At this circumstance, the LBB condition cannot be satisfied.
 - As $n_h < n_p \leq n_c$, the β_1 equals to zero, the β is bounded appended with h . However, considering both the first and second lines of Eq. (54), the reminder Ch^k in first line is not so small and should not be ignored due to $\ker \mathcal{P}_h \mathcal{I}_h \subset \ker P$ and $\beta_2 \neq 0$. It will lead to that β depend on h , $1 + \frac{C}{\beta} \approx 1$, thus, from the Eqs. (A.9), (A.20), the solution error will not be polluted by volumetric locking. [19]

327 This case is the typical spurious pressure mode or checkbox mode, a series
 328 of stabilization [50] is proposed to make $\ker \mathcal{P}\mathcal{I}_h = \ker \mathcal{P}$ to eliminate the
 329 spurious pressure mode.

- 330 • As $n_p \leq n_c$, $(V_{n_u} \setminus \ker \mathcal{P}\mathcal{I}_h) \subseteq (V_{n_u} \setminus \ker \mathcal{P}) \subseteq (V_{n_u} \setminus \mathcal{P})$, now, β is a
 331 constant independent with h, s .

332 Consequently, the dofs of pressure should remain $n_p \leq n_h$ or $n_p \leq n_c$ with a
 333 stabilizer to release the locking burden. Nevertheless, the value of n_h is hard to
 334 determine in practice, so the subgrid scale model [24] is introduced in this work
 335 as a stabilization. And n_c can be regarded as the optimal number of optimal
 336 volumetric constraint.

337 *4.2. Polynomial-wise constraint counting*

338 For now, n_c can be considered as the optimal pressure's dofs, and the way
 339 to determine n_c is shown as follows. For instance, in two dimensional nearly-
 340 incompressible elasticity problem, for linear polynomial space with dimension is
 341 3 namely P_3 , the counterpart displacement space V_3 is given by:

$$V_3 = \text{span} \left\{ \begin{pmatrix} 1 \\ 0 \end{pmatrix}, \begin{pmatrix} 0 \\ 1 \end{pmatrix}, \begin{pmatrix} x \\ 0 \end{pmatrix}, \begin{pmatrix} 0 \\ x \end{pmatrix}, \begin{pmatrix} y \\ 0 \end{pmatrix}, \begin{pmatrix} 0 \\ y \end{pmatrix} \right\} \quad (59)$$

342 or rearranged as follows,

$$V_3 = \text{span} \left\{ \underbrace{\begin{pmatrix} 1 \\ 0 \end{pmatrix}, \begin{pmatrix} 0 \\ 1 \end{pmatrix}, \begin{pmatrix} y \\ 0 \end{pmatrix}, \begin{pmatrix} 0 \\ x \end{pmatrix}, \begin{pmatrix} x \\ -y \end{pmatrix}}_{\ker \mathcal{P}}, \underbrace{\begin{pmatrix} x \\ y \end{pmatrix}}_{V_3 \setminus \ker \mathcal{P}} \right\} \quad (60)$$

343 It can be found from Eq. (60), for $n_u = 3$, $n_c = 1$. Following the path, the
 344 displacement space with quadratic polynomial base namely V_6 can be stated as:

$$V_6 = \text{span} \left\{ \underbrace{\begin{pmatrix} 1 \\ 0 \end{pmatrix}, \begin{pmatrix} 0 \\ 1 \end{pmatrix}, \begin{pmatrix} y \\ 0 \end{pmatrix}, \begin{pmatrix} 0 \\ x \end{pmatrix}, \begin{pmatrix} x \\ -y \end{pmatrix}, \begin{pmatrix} x^2 \\ -2xy \end{pmatrix}, \begin{pmatrix} y^2 \\ 0 \end{pmatrix}, \begin{pmatrix} 0 \\ x^2 \end{pmatrix}, \begin{pmatrix} -2xy \\ y^2 \end{pmatrix}}_{\ker \mathcal{P}}, \underbrace{\begin{pmatrix} x \\ y \end{pmatrix}, \begin{pmatrix} x^2 \\ 2xy \end{pmatrix}, \begin{pmatrix} 2xy \\ y^2 \end{pmatrix}}_{V_6 \setminus \ker \mathcal{P}} \right\} \quad (61)$$

345 In this circumstance, $n_c = 3$. As the order of polynomial space increasing, the
 346 every optimal numbers of constraint dofs for each order are listed in Table. 1.
 347 For the flexibility of usage, the relation between n_u and n_c is summarized as
 348 follows:

$$n_c = \frac{2n_u + 1 - \sqrt{1 + 8n_u}}{2} \quad (62)$$

349

Table 1: Degrees of freedom and volumetric constraint

Order of P_{n_u}	$2n_u$	n_c
1	6	1
2	12	3
3	20	6
4	30	10
\vdots	\vdots	\vdots
n	$(n+1)(n+2)$	$\frac{n(n+1)}{2}$

350 **5. FEM–meshfree mixed–formulation with optimal constraint**

351 *5.1. Finite element and reproducing kernel approximations*

352 In the proposed mixed-formulation, the displacement is approximated using
 353 three-node, six-node triangular elements and four-node, eight-node quadrilateral
 354 elements [1]. In order to flexcially adjust to let the dofs of pressure meets
 355 to be optimal, the reproducing kernel meshfree approximation is involved to
 356 approximate pressure.

357 In accordance with the reproducing kernel approximation, the entire domain
 358 Ω is discretized by n_p meshfree points, $\{\mathbf{x}_I\}_{I=1}^{n_p}$. Each meshfree point equips
 359 a meshfree shape function Ψ_I and nodal coefficient p_I , and the approximated
 360 pressure namely p_h can be presented by:

$$p_h(\mathbf{x}) = \sum_{I=1}^{n_p} \Psi_I(\mathbf{x}) p_I \quad (63)$$

361 where, in the reproducing kernel approximation framework, the shape function
 362 Ψ_I is given by:

$$\Psi_I(\mathbf{x}) = \mathbf{c}(\mathbf{x}_I - \mathbf{x}) \mathbf{p}(\mathbf{x}_I - \mathbf{x}) \phi(\mathbf{x}_I - \mathbf{x}) \quad (64)$$

363 in which \mathbf{p} is the basis function, especially for 2D quadratic basis function,
 364 having the following form:

$$\mathbf{p}(\mathbf{x}) = \{1, x, y, x^2, xy, y^2\}^T \quad (65)$$

365 and ϕ stands for the kernel function. In this work, the traditional Cubic B-spline
 366 function with square suppot is used as the kernel function:

$$\phi(\mathbf{x}_I - \mathbf{x}) = \phi(s_x) \phi(s_y), \quad s_i = \frac{\|\mathbf{x}_I - \mathbf{x}\|}{\bar{s}_{iI}} \quad (66)$$

367 with

$$\phi(s) = \frac{1}{3!} \begin{cases} (2-2s)^3 - 4(1-2s)^3 & s \leq \frac{1}{2} \\ (2-2s)^3 & \frac{1}{2} < s < 1 \\ 0 & s > 1 \end{cases} \quad (67)$$

368 where \bar{s}_{iI} 's are the support size towards the i -direction for the shape function Ψ_I .
 369 The correction function \mathbf{c} can be determined by the following so-call consistency
 370 condition:

$$\sum_{I=1}^{n_p} \Psi_I(\mathbf{x}) \mathbf{p}(\mathbf{x}_I) = \mathbf{p}(\mathbf{x}) \quad (68)$$

371 or equivalent shifted form:

$$\sum_{I=1}^{n_p} \Psi_I(\mathbf{x}) \mathbf{p}(\mathbf{x}_I - \mathbf{x}) = \mathbf{p}(\mathbf{0}) \quad (69)$$

³⁷² Substituting Eq. 64 into Eq. (??) leads to:

$$\mathbf{c}(\mathbf{x}_I - \mathbf{x}) = \mathbf{A}^{-1}(\mathbf{x}_I - \mathbf{x})\mathbf{p}(\mathbf{0}) \quad (70)$$

³⁷³ in which \mathbf{A} is namely moment matrix evaluating by:

$$\mathbf{A}(\mathbf{x}_I - \mathbf{x}) = \sum_{I=1}^{n_p} \mathbf{p}(\mathbf{x}_I - \mathbf{x}) \mathbf{p}^T(\mathbf{x}_I - \mathbf{x}) \phi(\mathbf{x}_I - \mathbf{x}) \quad (71)$$

³⁷⁴ Taking Eq. (70) back to Eq. (64), the final form of reproducing kernel shape
³⁷⁵ function can be got as:

$$\Psi_I(\mathbf{x}) = \mathbf{p}^T(\mathbf{0}) \mathbf{A}^{-1}(\mathbf{x}_I - \mathbf{x}) \phi(\mathbf{x}_I - \mathbf{x}) \quad (72)$$

³⁷⁶ 5.2. Bubble mesh generator

³⁷⁷ The proposed method embeds the optimal pressure DOFs to release the
³⁷⁸ burden of volumetric locking. In order to maintain the number of pressure
³⁷⁹ DOFs to be optimal, $n_p = n_c$, the Shimada method or namely bubble meshing
³⁸⁰ method is used to generate the pressure nodes. In Shimada method, as shown
³⁸¹ in Figure 2, a meshing node \mathbf{x}_I is regard as a bubble with specific radius r_I
³⁸² and mass m_I , the corresponding nodal location are determined by a dynamic
³⁸³ system as follows:

$$m_I \ddot{\mathbf{x}}_I + c_I \dot{\mathbf{x}}_I = \sum_{J=1}^{n_p} \bar{\mathbf{f}}_{IJ} \quad (73)$$

³⁸⁴ where the dot notion over the \mathbf{x} means to the time derivation of \mathbf{x} , i.e. $\dot{\mathbf{x}}_I, \ddot{\mathbf{x}}_I$
³⁸⁵ stands for the \mathbf{x}_I 's acceleration and velocity. The parameters m_I, c_I dnotes
³⁸⁶ mass and viscosity of the bubble at \mathbf{x}_I , and, for a better meshing efficiency and
³⁸⁷ stability, these two parameters are obtained through [51]:

$$k = \frac{1.47}{2r_I}, \quad \zeta = \frac{c_I}{2\sqrt{m_I k}} = 0.7 \quad (74)$$

³⁸⁸ The interaction forces between adjacent bubbles $\bar{\mathbf{f}}_{IJ}$'s is given by:

$$\bar{\mathbf{f}}_{IJ} = \frac{\mathbf{x}_I - \mathbf{x}_J}{d_{IJ}} \bar{f}_{IJ}, \quad \bar{f}_{IJ} = \begin{cases} (1 - w^4)e^{-w^4} & 0 \leq w = \frac{d_{IJ}}{r_I + r_J} \leq 1.5 \\ 0 & w > 1.5 \end{cases} \quad (75)$$

³⁸⁹ where $d_{IJ} = \|\mathbf{x}_I - \mathbf{x}_J\|$ denotes the distance between \mathbf{x}_I and \mathbf{x}_J .

³⁹⁰ Subsequently, the locations \mathbf{x}_I 's can be got by solve the above Eq. (74)
³⁹¹ using conventional fourth-order Runge-Kutta method.

³⁹² As shown in Figure. 2, the detailed meshing steps are listed as follows:

- ³⁹³ 1. Generate the elements for displacement using traditional meshing algo-
³⁹⁴ rithm, for example Frontal-Delaunay algorithm , where the number of the
³⁹⁵ displacement nodes is n_u .

- 396 2. Arrange the fixed pressure nodes on the boundary before locating nodes
 397 in the domain, and the bubbles of the boundary nodes should cover all
 398 boundaries to avoid the internal nodes escaping out.
 399 3. Place a specific number of nodes in the domain and let the total number of
 400 pressure nodes equal to optimal one based on the number of displacement
 401 nodes, i.e. $n_p = n_c(n_u)$.
 402 4. Determine the locations of the nodes generated by Step. 3 via solving Eq.
 403 (73) using fourth-order Runge-Kutta method.

404 In this mixed approximation, due to the locality of finite element shape
 405 functions and the globality of meshfree shape functions, the numerical integra-
 406 tion for assembling the stiffness matrices is carried out in the elements of finite
 407 element approximation. The previous works have figured out that, the overlap-
 408 ping supports and the rational property of meshfree shape functions will cause
 409 a mismatch between shape function and its derivate in the procedure of the nu-
 410 merical integration by parts. This phenomenon, namely integration constraint,
 411 will bring the lower accurate results, and can be alleviated using higher or-
 412 der Gaussian quadrature rules or more efficient consistent meshfree integration
 413 rules. However, there is no similar problems in proposed mixed-formulations for
 414 incompressible elasticity or heat diffusion problems, since only meshfree shape
 415 functions are adopted in weak forms of Eqs. (??). So just using the lower order
 416 Gaussian quadrature rules used in traditional finite element method can meet
 417 the accuracy requirement.

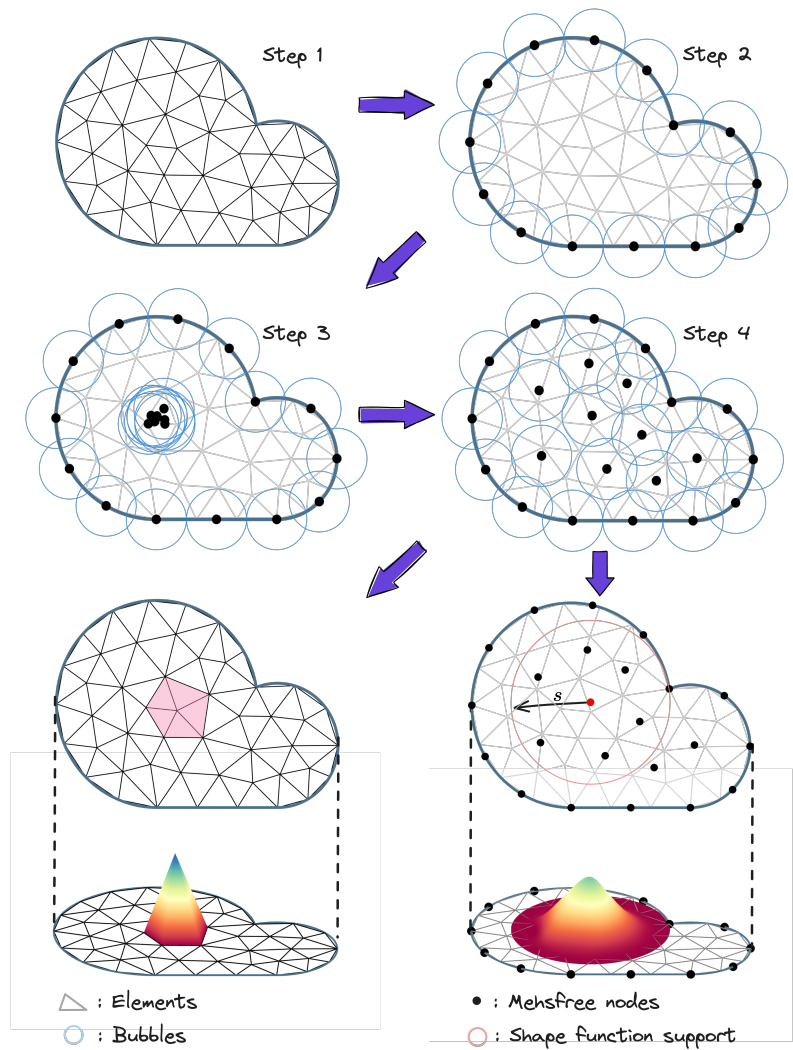


Figure 2: Illustration of mesh generation for finite element and meshfree mixed approximations

⁴¹⁸ **6. Numerical examples**

⁴¹⁹ *6.1. Inf-sup test*

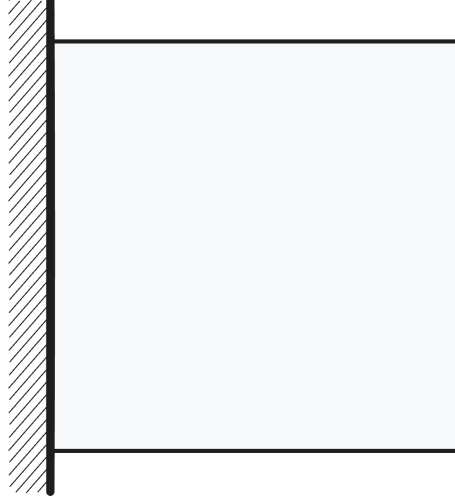


Figure 3: Illustration of inf-sup test

⁴²⁰ *6.1.1. Inf-sup test*

Table 2: Results of Nearly-incompressible elasticity patch test

	Linear patch test		Quadratic patch test	
	L_2 -Error	H_e -Error	L_2 -Error	H_e -Error
T3-stripe				
T3-cross				
T3-mix				
Q4				
Q4R1				
Q4-mix				
T6				
T6P3				
T6-mix				
Q8				
Q8P3				
Q8-mix				

⁴²¹ *6.2. Cantilever beam problem*

⁴²² *6.3. Plate with hole problem*

⁴²³ *6.4. Cook membrane problem*

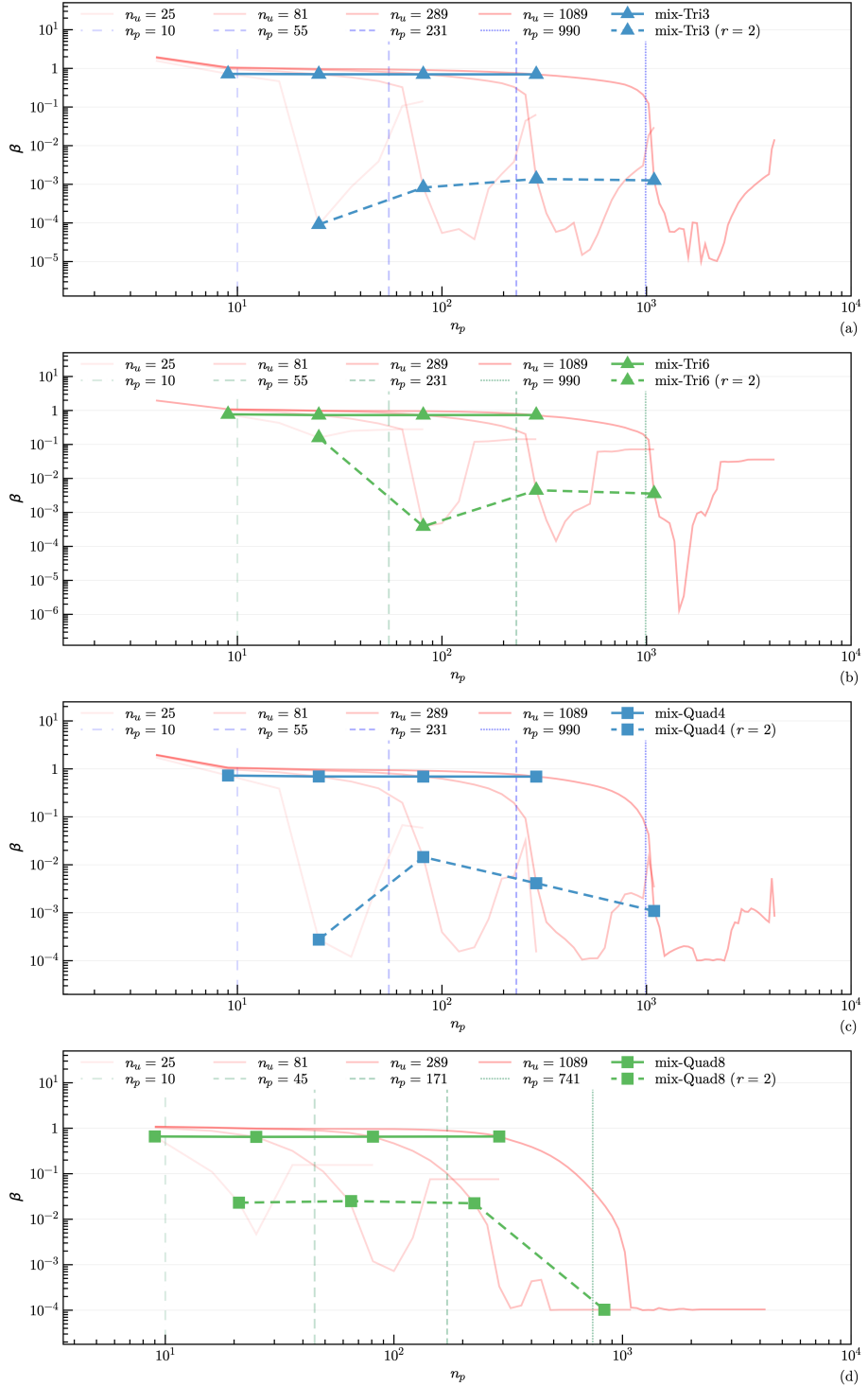


Figure 4: Inf-sup test for various finite element formulations:
(a) mix-Tri3; (b) mix-Tri6; (c) mix-Quad4; (d) mix-Quad8

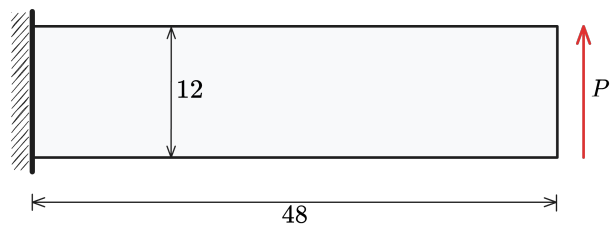


Figure 5: Illustration of cantilever beam problem

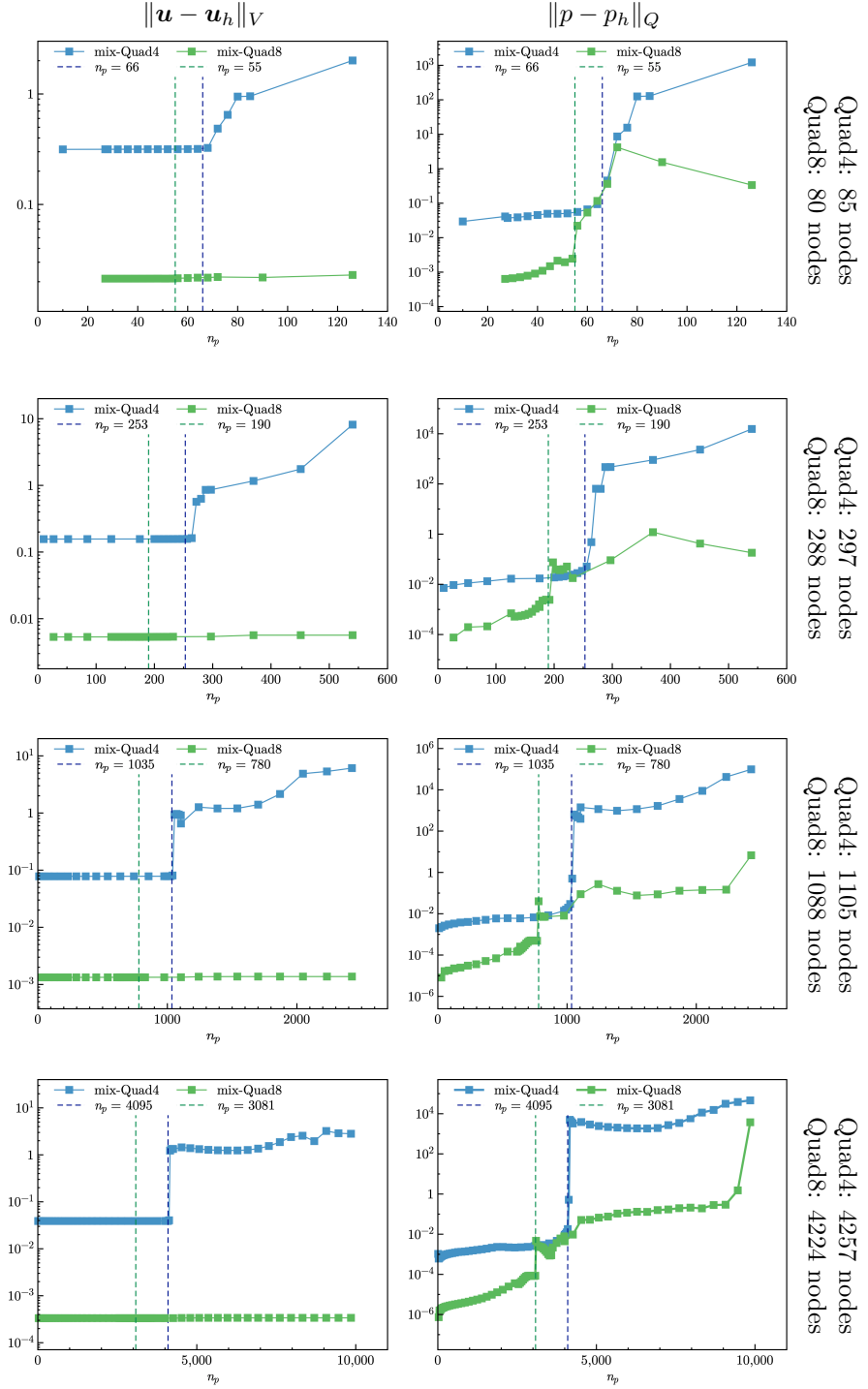


Figure 6

Figure 7: Contour plots of cantilever beam problem

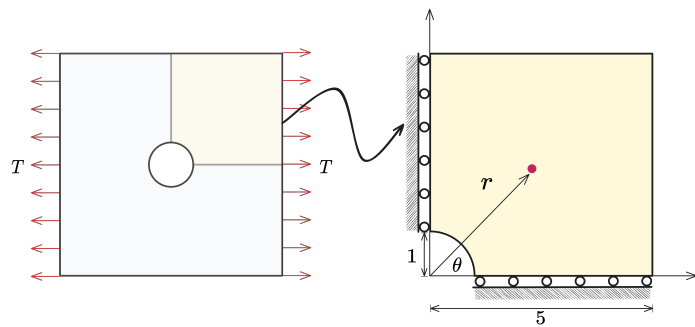


Figure 8: Illustration of plate with hole problem

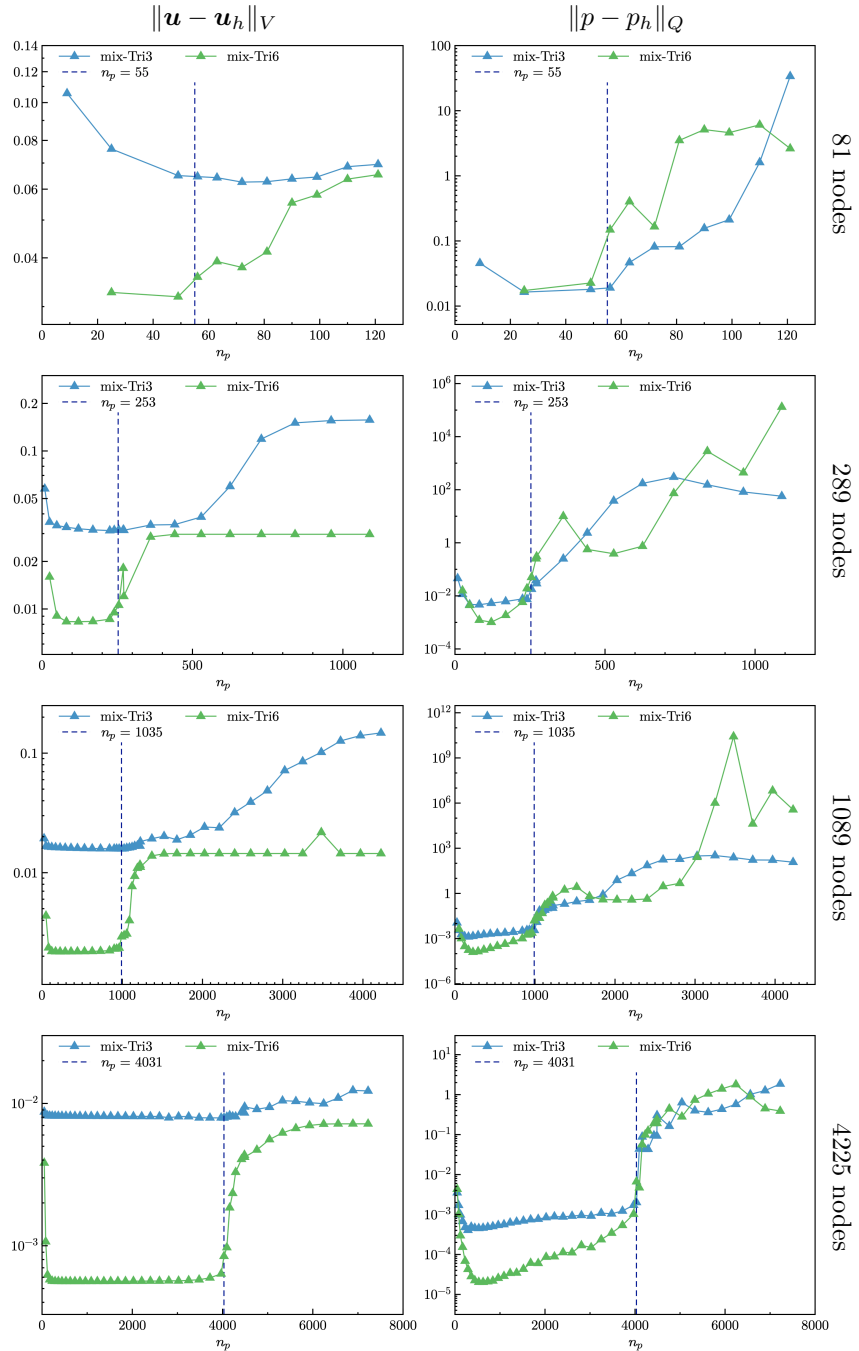


Figure 9

Figure 10: Contour plots of cantilever beam problem

Figure 11: Convergence comparison of cook membrane problem

Figure 12: Contour plots of cook membrane problem

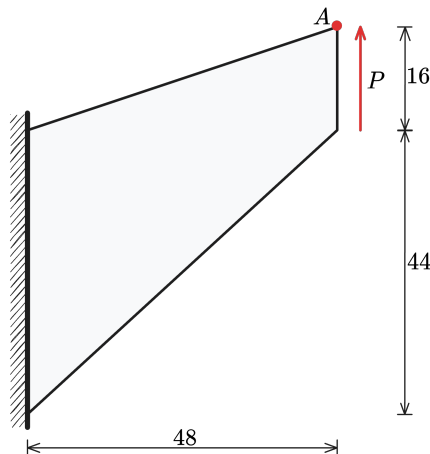


Figure 13: Illustration of cook membrane problem

Figure 14: Illustration of block under compression problem

Figure 15: Convergence comparison of block under compression problem

Figure 16: Contour plots of block under compression problem

424 **References**

- 425 [1] T. J. Hughes, The Finite Element Method: Linear Static and Dynamic
426 Finite Element Analysis, Prentice Hall, New Jersey, 2000.
- 427 [2] I. Babuška, R. Narasimhan, The Babuška-Brezzi condition and the patch
428 test: An example, Computer Methods in Applied Mechanics and Engineering 140 (1997) 183–199.
- 430 [3] K. J. Bathe, Finite Element Procedures, Prentice Hall, Englewood Cliffs,
431 New Jersey, 1996.
- 432 [4] D. S. Malkus, Eigenproblems associated with the discrete LBB condition for
433 incompressible finite elements, International Journal of Engineering Science 19 (1981) 1299–1310.
- 435 [5] D. Chapelle, K. J. Bathe, The inf-sup test, Computers & Structures 47
436 (1993) 537–545.
- 437 [6] F. Brezzi, K. J. Bathe, Studies of finite element procedures the inf-sup
438 condition equivalent forms and applications.
- 439 [7] D. Gallistl, Rayleigh–Ritz approximation of the inf-sup constant for the
440 divergence, Mathematics of Computation 88 (2019) 73–89.
- 441 [8] P. Hood, C. Taylor, Navier-Stokes equations using mixed interpolation,
442 Finite element methods in flow problems (1974) 121–132.
- 443 [9] D. S. Malkus, T. J. Hughes, Mixed finite element methods - Reduced and
444 selective integration techniques: A unification of concepts, Computer Meth-
445 ods in Applied Mechanics and Engineering 15 (1978) 63–81.
- 446 [10] T. Shilt, R. Deshmukh, J. J. McNamara, P. J. O’Hara, Solution of nearly
447 incompressible field problems using a generalized finite element approach,
448 Computer Methods in Applied Mechanics and Engineering 368 (2020)
449 113165.
- 450 [11] J. C. Simo, M. S. Rifai, A class of mixed assumed strain methods and
451 the method of incompatible modes, International Journal for Numerical
452 Methods in Engineering 29 (1990) 1595–1638.
- 453 [12] M. Broccardo, M. Micheloni, P. Krysl, Assumed-deformation gradient finite
454 elements with nodal integration for nearly incompressible large deformation
455 analysis, International Journal for Numerical Methods in Engineering 78
456 (2009) 1113–1134.
- 457 [13] W. M. Coombs, T. J. Charlton, M. Cortis, C. E. Augarde, Overcoming vol-
458 umetric locking in material point methods, Computer Methods in Applied
459 Mechanics and Engineering 333 (2018) 1–21.

- 460 [14] S. Saloustros, M. Cervera, S. Kim, M. Chiumenti, Accurate and locking-free
461 analysis of beams, plates and shells using solid elements, Computational
462 Mechanics (Jan. 2021).
- 463 [15] C. Rodriguez, T.-H. Huang, A variationally consistent reproducing kernel
464 enhanced material point method and its applications to incompressible
465 materials, Computational Mechanics (2023) 1–20.
- 466 [16] J. Simo, R. Taylor, K. Pister, Variational and projection methods for the
467 volume constraint in finite deformation elasto-plasticity, Computer Methods
468 in Applied Mechanics and Engineering 51 (1985) 177–208.
- 469 [17] C. R. Dohrmann, P. B. Bochev, A stabilized finite element method for the
470 Stokes problem based on polynomial pressure projections, International
471 Journal for Numerical Methods in Fluids 46 (2004) 183–201.
- 472 [18] C. Lovadina, F. Auricchio, On the enhanced strain technique for elasticity
473 problems, Computers & Structures 81 (2003) 777–787.
- 474 [19] K.-J. Bathe, The inf-sup condition and its evaluation for mixed finite ele-
475 ment methods, Computers & Structures 79 (2001) 243–252.
- 476 [20] T. J. R. Hughes, Multiscale phenomena: Green's functions, the Dirichlet-
477 to-Neumann formulation, subgrid scale models, bubbles and the origins of
478 stabilized methods, Computer Methods in Applied Mechanics and Engi-
479 neering 127 (1995) 387–401.
- 480 [21] A. Masud, K. Xia, A Stabilized MixedFinite Element Method for Nearly
481 IncompressibleElasticity, Journal of Applied Mechanics 72 (2005) 711–720.
- 482 [22] R. Rossi, R. Zorrilla, R. Codina, A stabilised displacement-volumetric
483 strain formulation for nearly incompressible and anisotropic materials,
484 Computer Methods in Applied Mechanics and Engineering 377 (2021)
485 113701.
- 486 [23] E. Karabelas, M. A. F. Gsell, G. Haase, G. Plank, C. M. Augustin, An
487 accurate, robust, and efficient finite element framework with applications to
488 anisotropic, nearly and fully incompressible elasticity, Computer Methods
489 in Applied Mechanics and Engineering 394 (2022) 114887.
- 490 [24] T. J. R. Hughes, L. P. Franca, M. Balestra, A new finite element formu-
491 lation for computational fluid dynamics: V. Circumventing the babuška-
492 brezzi condition: A stable Petrov-Galerkin formulation of the stokes prob-
493 lem accommodating equal-order interpolations, Computer Methods in Ap-
494 plied Mechanics and Engineering 59 (1986) 85–99.
- 495 [25] D. N. Arnold, F. Brezzi, M. Fortin, A stable finite element for the Stokes
496 equations, CALCOLO 21 (1984) 337–344.

- 497 [26] F. Auricchio, L. Beirão da Veiga, C. Lovadina, A. Reali, A stability study of
 498 some mixed finite elements for large deformation elasticity problems, Computer Methods in Applied Mechanics and Engineering 194 (2005) 1075–
 499 1092.
- 501 [27] A. Quarteroni, A. Valli, Numerical Approximation of Partial Differential
 502 Equations, Springer Series in Computational Mathematics, Springer,
 503 Berlin, 1994.
- 504 [28] M. Crouzeix, P. Raviart, Conforming and nonconforming finite element
 505 methods for solving the stationary Stokes equations I, Revue française
 506 d'automatique informatique recherche opérationnelle. Mathématique 7
 507 (1973) 33–75.
- 508 [29] U. Brink, E. Stein, On some mixed finite element methods for incompressible
 509 and nearly incompressible finite elasticity, Computational Mechanics
 510 19 (1996) 105–119.
- 511 [30] T. Belytschko, Y. Y. Lu, L. Gu, Element-free Galerkin methods, International
 512 Journal for Numerical Methods in Engineering 37 (1994) 229–256.
- 513 [31] W. K. Liu, S. Jun, Y. F. Zhang, Reproducing kernel particle methods,
 514 International Journal for Numerical Methods in Fluids 20 (1995) 1081–
 515 1106.
- 516 [32] S. W. Chi, J. S. Chen, H. Y. Hu, A weighted collocation on the strong form
 517 with mixed radial basis approximations for incompressible linear elasticity,
 518 Computational Mechanics 53 (2014) 309–324.
- 519 [33] L. Wang, Z. Qian, Y. Zhou, Y. Peng, A weighted meshfree collocation
 520 method for incompressible flows using radial basis functions, Journal of
 521 Computational Physics 401 (2020) 108964.
- 522 [34] A. Ortiz-Bernardin, M. Puso, N. Sukumar, Improved robustness for nearly-
 523 incompressible large deformation meshfree simulations on Delaunay tes-
 524 sellations, Computer Methods in Applied Mechanics and Engineering 293
 525 (2015) 348–374.
- 526 [35] T. J. Hughes, J. A. Cottrell, Y. Bazilevs, Isogeometric analysis: CAD,
 527 finite elements, NURBS, exact geometry and mesh refinement, Computer
 528 Methods in Applied Mechanics and Engineering 194 (2005) 4135–4195.
- 529 [36] F. Auricchio, L. Beirão da Veiga, C. Lovadina, A. Reali, The importance
 530 of the exact satisfaction of the incompressibility constraint in nonlinear
 531 elasticity: Mixed FEMs versus NURBS-based approximations, Computer
 532 Methods in Applied Mechanics and Engineering 199 (2010) 314–323.
- 533 [37] A. Huerta, S. Fernández-Méndez, Locking in the incompressible limit for
 534 the element-free Galerkin method, International Journal for Numerical
 535 Methods in Engineering 51 (2001) 1361–1383.

- 536 [38] J. Dolbow, T. Belytschko, Volumetric locking in the element free Galerkin
 537 method, International Journal for Numerical Methods in Engineering 46
 538 (1999) 925–942.
- 539 [39] G. Moutsanidis, J. J. Koester, M. R. Tupek, J.-S. Chen, Y. Bazilevs, Treatment
 540 of near-incompressibility in meshfree and immersed-particle methods,
 541 Computational Particle Mechanics 7 (2020) 309–327.
- 542 [40] G. Moutsanidis, W. Li, Y. Bazilevs, Reduced quadrature for FEM, IGA
 543 and meshfree methods, Computer Methods in Applied Mechanics and En-
 544 gineering 373 (2021) 113521.
- 545 [41] Z.-Y. Wang, Y.-F. Jin, Z.-Y. Yin, Y.-Z. Wang, Overcoming volumetric
 546 locking in stable node-based smoothed particle finite element method with
 547 cubic bubble function and selective integration, International Journal for
 548 Numerical Methods in Engineering 123 (2022) 6148–6169.
- 549 [42] J. S. Chen, S. Yoon, H. P. Wang, W. K. Liu, An improved reproducing
 550 kernel particle method for nearly incompressible finite elasticity, Computer
 551 Methods in Applied Mechanics and Engineering 181 (2000) 117–145.
- 552 [43] C. M. Goh, P. M. F. Nielsen, M. P. Nash, A stabilised mixed mesh-
 553 free method for incompressible media: Application to linear elasticity and
 554 Stokes flow, Computer Methods in Applied Mechanics and Engineering 329
 555 (2018) 575–598.
- 556 [44] D. S. Bombarde, M. Agrawal, S. S. Gautam, A. Nandy, Hellinger–Reissner
 557 principle based stress–displacement formulation for three-dimensional iso-
 558 geometric analysis in linear elasticity, Computer Methods in Applied Me-
 559 chanics and Engineering 394 (2022) 114920.
- 560 [45] A. Huerta, Y. Vidal, P. Villon, Pseudo-divergence-free element free
 561 Galerkin method for incompressible fluid flow, Computer Methods in Ap-
 562 plied Mechanics and Engineering 193 (2004) 1119–1136.
- 563 [46] C. Wu, W. Hu, J. Chen, A meshfree-enriched finite element method for
 564 compressible and near-incompressible elasticity, International Journal for
 565 Numerical Methods in Engineering 90 (2012) 882–914.
- 566 [47] C. Philippe G., Linear and Nonlinear Functional Analysis with Applica-
 567 tions, SIAM-Society for Industrial and Applied Mathematics, Philadelphia,
 568 2013.
- 569 [48] I. Babuška, J. Osborn, Eigenvalue Problems, in: Handbook of Numerical
 570 Analysis, Vol. 2 of Finite Element Methods (Part 1), Elsevier, 1991, pp.
 571 641–787.
- 572 [49] K. Yosida, Functional Analysis, 6th Edition, Classics in Mathematics,
 573 Springer-Verlag, Berlin Heidelberg, 1995.

- 574 [50] B. Vadala-Roth, S. Acharya, N. A. Patankar, S. Rossi, B. E. Griffith, Sta-
575 bilization approaches for the hyperelastic immersed boundary method for
576 problems of large-deformation incompressible elasticity, Computer Meth-
577 ods in Applied Mechanics and Engineering 365 (2020) 112978.
- 578 [51] V. Q. Dinh, Y. Marechal, GPU-based parallelization for bubble mesh gen-
579 eration, COMPEL - The international journal for computation and math-
580 ematics in electrical and electronic engineering 36 (2017) 1184–1197.
- 581 [52] S. C. Brenner, L. R. Scott, The Mathematical Theory of Finite Element
582 Methods, Springer, New York, 2008.
- 583 [53] D. N. Arnold, L. R. Scott, M. Vogelius, Regular Inversion of the Divergence
584 Operator with Dirichlet Boundary Conditions on a Polygon, Institute for
585 Mathematics and its Applications (USA), 1987.

586 **Appendix A. Error estimator for mixed-formulation**

587 In this appendix, the traditional error estimators for mixed-formulation are
 588 illustrated herein, the proof is referred to [52]. The weak formula for mixed-
 589 formulation is given by: find $u_h \in V_h, p_h \in Q_h$,

$$\begin{aligned} a(v_h, u_h) + b(v_h, p_h) &= f(v_h), \quad \forall v_h \in V_h \\ b(u_h, q_h) &= g(q_h), \quad \forall q_h \in Q_h \end{aligned} \quad (\text{A.1})$$

590 The error estimator of Eq. (A.1) is presented under two cases, $g(q_h) = 0$ or
 591 $g(q_h) \neq 0$ for all $q_h \in Q_h$.

592 For $g(q_h) = 0$, the variational problem (A.1) becomes to the following equiv-
 593 alent one: find $u_h \in Z_h^0$,

$$u_h \in Z_h^0 \quad a(v_h, u_h) = f(v_h), \quad \forall v_h \in Z_h^0 \quad (\text{A.2})$$

594 where $Z_h^0 = \ker P_h \subset V_h$. The bilinear form a covers the continuity, coercivity
 595 and orthogonality on space Z_h^0 , thus the following Céa inequality [52] should be
 596 held true:

$$\|u - u_h\|_V \leq \frac{C}{\alpha} \inf_{w_h \in Z_h^0} \|u - w_h\|_V \quad (\text{A.3})$$

597 Furthermore, suppose $v_h \in V_h$ to satisfy that:

$$\inf_{q_h \in Q_h} \frac{b(w_h - v_h, q_h)}{\|w_h - v_h\|_V \|q_h\|_Q} = \inf_{q_h \in Q_h} \sup_{v'_h \in V_h} \frac{b(v'_h, q_h)}{\|v'_h\|_V \|q_h\|_Q} = \beta \quad (\text{A.4})$$

598 or

$$\|w_h - v_h\|_V = \frac{1}{\beta} \inf_{q_h \in Q_h} \frac{b(w_h - v_h, q_h)}{\|q_h\|_Q} \quad (\text{A.5})$$

599 According to $u, w_h \in Z_h^0$ leads to following orthogonality for b :

$$b(u - w_h, q_h) = 0, \quad \forall q_h \in Q_h \quad (\text{A.6})$$

600 Thus, with the combination of Eqs. (A.5), (A.6) and continuity of b yields:

$$\begin{aligned} \|v_h - w_h\|_V &= \frac{1}{\beta} \inf_{q_h \in Q_h} \frac{b(w_h - v_h, q_h)}{\|q_h\|_Q} && \text{(Eq.(A.5))} \\ &= \frac{1}{\beta} \inf_{q_h \in Q_h} \frac{b(w_h - v_h, q_h) + b(u - w_h, q_h)}{\|q_h\|_Q} && \text{(orthogonality)} \\ &= \frac{1}{\beta} \inf_{q_h \in Q_h} \frac{b(u - v_h, q_h)}{\|q_h\|_Q} \\ &\leq \frac{C}{\beta} \|u - v_h\|_V && \text{(continuity)} \end{aligned} \quad (\text{A.7})$$

601 then

$$\|u - w_h\|_V \leq \|u - v_h\|_V + \|v_h - w_h\|_V \leq (1 + \frac{C}{\beta}) \|u - v_h\|_V \quad (\text{A.8})$$

602 Finally, plugging Eq. (A.8) into Eq. (A.3), the error estimator for the case
603 of $g(q_h) = 0$, $\forall q_h \in Q_h$ turns to that:

$$\|u - u_h\|_V \leq \frac{C}{\alpha} \inf_{w_h \in Z_h} \|u - w_h\|_V \leq \frac{C}{\alpha} \left(1 + \frac{C}{\beta}\right) \inf_{v_h \in V_h} \|u - v_h\|_V \quad (\text{A.9})$$

604 For the problem with $g(q) \neq 0$, $\forall q \in Q$, the u_h can be split into two parts,
605 $u_h = u_h^0 + u_h^g$, where $u_h^0 \in Z_h^0$ [53]. Now, the problem of variational problem
606 becomes the following equivalent form: find $u_h^0 \in Z_h^0$,

$$a(v_h, u_h^0) = f(v_h) - a(v_h, u_h^g), \quad \forall v_h \in Z_h^0 \quad (\text{A.10})$$

607 Under this circumstance, it obviously has the following relationship:

$$b(u_h^0, q_h) = b(u_h - u_h^g, q_h) = 0 \Rightarrow b(u_h, q_h) = b(u_h^g, q_h) = g(q_h), \quad \forall q_h \in Q_h \quad (\text{A.11})$$

608 and then $u_h, u_h^g \in Z_h$. For a result, the coercivity for bilinear form turns to
609 that:

$$\alpha \|v_h\|_V \leq \sup_{w_h \in Z_h^0} \frac{a(v_h, w_h)}{\|w_h\|_V}, \quad \forall v_h \in Z_h \quad (\text{A.12})$$

610 As $Z_h^0 \not\subseteq Z_h$, the orthogonality and Céa inequality is no longer held true, the
611 error estimator is bounded by the following [52]:

$$\|u - u_h\|_V \leq \left(1 + \frac{C}{\alpha}\right) \inf_{w_h \in Z_h} \|u - w_h\|_V + \frac{1}{\alpha} \sup_{w_h^0 \in Z_h^0} \frac{|a(u - u_h, w_h^0)|}{\|w_h^0\|_V} \quad (\text{A.13})$$

612 Since $Z_h^0 \subset V_h$,

$$a(w_h^0, u) + b(w_h^0, p) = f(w_h^0), \quad \forall w_h^0 \in Z_h^0 \quad (\text{A.14})$$

613 With a subtraction between Eq. (A.14) and Eq. (A.10) and the definition of
614 space Z_h^0 , we have:

$$a(w_h^0, u - u_h) + b(w_h^0, p - q_h) = 0, \quad \forall w_h^0 \in Z_h^0, \quad \forall q_h \in Q_h \quad (\text{A.15})$$

615 thus,

$$|a(u - u_h, w_h^0)| = |b(w_h^0, p - q_h)| \leq C \|p - q_h\|_Q \|w_h^0\|_V, \quad \forall w_h^0 \in Z_h^0 \quad (\text{A.16})$$

616 Moreover, for $w_h \in Z_h^g$, let $v_h \in V_h$ satisfies that:

$$\|w_h - v_h\|_V = \frac{1}{\beta} \inf_{q_h \in Q_h} \frac{b(w_h - v_h, q_h)}{\|q_h\|_Q} \quad (\text{A.17})$$

617 Following the same path of Eq. (A.7) can obtain that:

$$\|v_h - w_h\|_V \leq \frac{C}{\beta} \|u - v_h\|_V \quad (\text{A.18})$$

⁶¹⁸ Thus, for $w_h \in Z_h$,

$$\|u - w_h\|_V \leq \|u - v_h\|_V + \|v_h - w_h\|_V \leq (1 + \frac{C}{\beta})\|u - v_h\|_V \quad (\text{A.19})$$

⁶¹⁹ Consequently, substituting Eqs. (A.16), (A.19) into Eq. (A.13) leads to:

$$\begin{aligned} \|u - u_h\|_V &\leq (1 + \frac{C}{\alpha}) \inf_{w_h \in Z_h} \|u - w_h\|_V + \frac{1}{\alpha} \sup_{w_h^0 \in Z_h^0} \frac{|a(u - u_h, w_h^0)|}{\|w_h^0\|_V} \\ &\leq (1 + \frac{C}{\alpha})(1 + \frac{C}{\beta}) \inf_{v_h \in V_h} \|u - v_h\|_V + \frac{C}{\alpha} \inf_{q_h \in Q_h} \|p - q_h\|_Q \end{aligned} \quad (\text{A.20})$$